Folded Loop Antenna for Mobile Hand-Held Units

Konstantinos D. Katsibas, Constantine A. Balanis, *Fellow, IEEE*,
Panayiotis A. Tirkas, *Member, IEEE*, and Craig R. Birtcher

***Abstract*— The vertical folded loop antenna, modeled as wire and printed radiating element mounted on a conducting box, simulating a cellular telephone with and without dielectric coating, is analyzed. Finite-difference time-domain (FDTD) method is used to calculate radiation patterns and input impedance. The results are compared with measurements and with NEC data. Very good agreement is obtained in all cases. Parasitic loading is used to enhance the bandwidth of the printed element. The antenna meets design requirements for existing and future mobile communication systems.**

***Index Terms*—Loop antennas, mobile antennas, portable radio communication.**

I. Introduction

WIRELESS communications, specifically cellular communications, is currently the fastest growing segment in the telecommunications industry and promises to become the preferred medium of telecommunications in the future. In recent years, there has been tremendous worldwide activity aimed to develop mobile communication systems. Currently, the most widely adopted systems are the Global System for Mobile (GSM) Communications [1] developed primarily in Europe and Asia and Interim Standard-54 (IS-54) [2], developed in North America (United States and Canada). The communication between the mobile station (MS) and base station (BS) is implemented through two links; uplink (MS to BS) and downlink (BS to MS). The frequency bands for GSM are 890–915 MHz and 935–960 MHz for the uplink and downlink, respectively, while for IS-54 they are 869–894 MHz for the uplink and 824–849 MHz for the downlink. The new generation of personal communication systems (PCS) (such as the DCS 1800) has frequency bands of 1.710–1.785 GHz and 1.805–1.880 GHz for the uplink and downlink, respectively.

Antennas used in mobile communications have been recognized as critical elements that can either enhance or constrain system performance. The effective design of mobile radiation elements mounted on hand-held units should meet specific requirements such as small size, light weight, low cost, attractive appearance and ease of construction. The antenna dimensions should be sufficiently small to be mounted on the limited space provided on the surface of the equipment. Radiation characteristics of such antenna systems usually differ from those of antenna elements radiating in free space. The radiation pattern varies depending on the size and composition of the unit, and the location of the antenna element. The desired radiation pattern of the antenna on the hand-held device should be primarily omnidirectional in the horizontal plane. The gain should be as large as possible and the resonant frequency should be within the operating band.

In recent years, simulation tools have been developed for analyzing radiation elements that would have desired characteristics. The monopole mounted on a hand-held unit, which was analyzed in [3] and [4], is the most widely used antenna element for mobile communications. However, since it can be easily broken it is not considered rigid. Other candidate antennas, like the conformal planar inverted F antenna (PIFA), have been proposed [4], [5]. Since the PIFA element is mounted on the side of the telephone, the hand position (holding the cellular phone) detunes the antenna resonant frequency and input impedance.

In this paper, the vertical folded loop antenna, designed both as wire and as printed radiation element on a dielectric substrate, is mounted on a conducting box with and without a dielectric coating. It is analyzed using the finite-difference time-domain (FDTD) method. The Berenger's perfectly matched layer (PML) [6] is used to truncate the FDTD computational domain. Past contributions in this area have demonstrated the effectiveness of the PML [7]–[9].

Results are given for a dielectric-covered conducting box to simulate a portable telephone with a plastic case surrounding the metal chassis. The radiation patterns and the input impedance for the folded loop antenna attached on the conducting box (with and without dielectric coating) are given. The FDTD results are compared with measurements and with predictions based on the numerical electromagnetics code (NEC) [10].

II. Approach

FDTD [11] is a popular technique that converts Maxwell's time-dependent curl equations into difference equations, which are then solved in a time-marching sequence by alternately calculating the electric and magnetic fields in an interlaced spatial grid. This was used successfully in the past for a variety of antenna configurations [12]–[14].

The solution of radiation problems requires the use of absorbing boundary conditions (ABC) to accurately terminate the computational domain, allow the propagation of electromagnetic waves out of the computational space, and reduce the reflections within the region of interest. Recently, a new ABC—the PML—has been introduced by Berenger [6]. The PML uses nonphysical absorbing material for the grid truncation, which matches the impedance of the medium to that of free-space for all angles of incidence and all frequencies.

Manuscript received April 15, 1996; revised May 20, 1997.

The authors are with the Department of Electrical Engineering, Telecommunications Research Center, Arizona State University, Tempe, AZ 85287 USA.

Publisher Item Identifier S 0018-926X(98)01495-1.

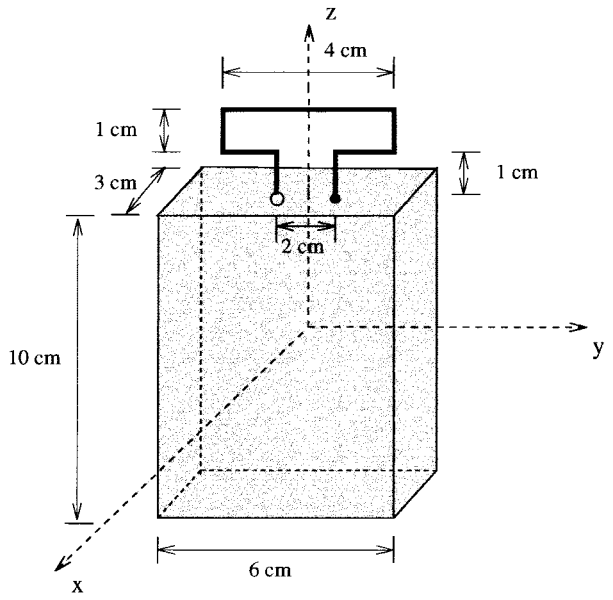

Fig. 1. Wire folded loop antenna mounted on a conducting box.

The conventional PML region requires that the FDTD field components be split into two orthogonal components.

The structure in the FDTD region should be enclosed by a near-to-far field transform surface. The electric and magnetic fields on this surface are used to implement a near-field to far-field transformation by utilizing the equivalence principle [15]. This is particularly useful when the radiation patterns in the far-field region of the antenna are examined.

The time-step Δt of the FDTD algorithm must be bounded by the space increments Δx, Δy, and Δz to avoid numerical instabilities. A typical time-step choice of Δt for $\Delta x = \Delta y = \Delta z$ is $\Delta t = \frac{\Delta x}{2c}$ [16], where c is the speed of light in free-space and Δx is the size of the cubic grid used.

The geometry of the first antenna to be analyzed is shown in Fig. 1. It is a conducting box with the loop element mounted on its top, and it simulates a small hand-held portable telephone. A second model that is analyzed is the conducting box coated with a dielectric material to simulate a portable telephone with a plastic case surrounding the metal chassis. The plastic layer is modeled as a lossless dielectric layer immediately adjacent to the conducting chassis with permittivity $\epsilon_r = 2.6$.

The finite-difference form of Maxwell's curl equations are derived based on a homogeneous region. Therefore, the air–dielectric interface points require special treatment. The field components which lie on the air–dielectric interface for the front box surface are the tangential components of $\vec{E}$ (E_y and E_z) and the normal component of $\vec{H}$ (H_x). In calculating H_x, the standard FDTD equations can still be used because the value of μ does not change across the boundary. To calculate E_y and E_z, however, a new finite-difference formulation must be derived from the field continuity conditions across the boundary. The tangential electric fields in cells that contain the dielectric must be modified.

A typical contour C_1 used to evaluate the tangential electric fields at the air–dielectric interface is shown in Fig. 2(a). It

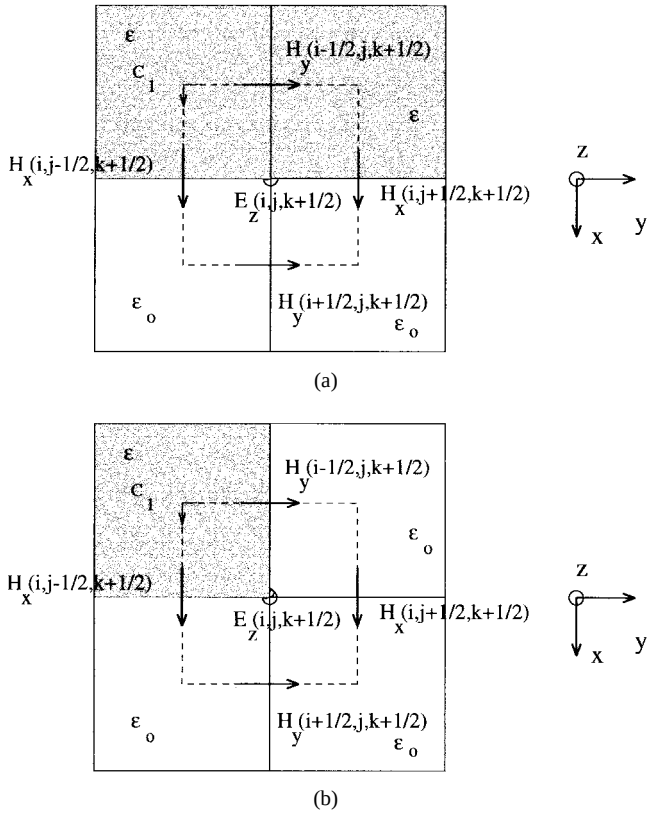

Fig. 2. Dielectric–air interface of the front box surface and edges within the FDTD computational domain.

is the top view of the air–dielectric interface of the front surface of the box. The dielectric coating of permittivity ϵ is represented by the shaded region and the air region with permittivity ϵ_o is shown beneath. By applying Ampere's Law in the air–dielectric interface of the front surface of the box, we can write

$$\oint H\,dl = \frac{\partial}{\partial t}\int_S \epsilon E\,ds = -\frac{\partial}{\partial t}(\epsilon_{\text{ave}} E_z\,ds) \tag{1}$$

where ϵ_{ave} represents the average dielectric permittivity $[\epsilon_{\text{ave}} = (\epsilon_o + \epsilon)/2]$ between the two media in the contour.

The edges of the box also require special treatment. In Fig. 2(b), the top view of the air–dielectric interfaces of one of the front edges of the box is illustrated. In this case, the contour C_1 encloses three cells with air of permittivity ϵ_o and one cell with dielectric material of permittivity ϵ. Ampere's law can be utilized again along the contour C_1 to update the tangential electric fields along the air–dielectric interface. Because at the edge $3/4$ of the cell is air and $1/4$ is dielectric, the average dielectric permittivity is now $\epsilon_{\text{ave}} = \frac{3\epsilon_o + \epsilon}{4}$. The same approach is used to evaluate the tangential electric fields on the air–dielectric interface for the remaining faces of the box.

The feed of the wire folded loop antenna was modeled using an equivalent magnetic-frill model [3], [17]. This was accomplished by defining the four electric field components on the top surface of the conducting box extending radially from the wire antenna axis. The source of excitation is a Rayleigh pulse, which is the derivative with respect to time of

a Gaussian pulse. Because of its smooth shaped spectrum, it provides information from dc to the desired frequency simply by adjusting the width of the pulse and allows wideband input impedance prediction with one computational run.

The input impedance of the antenna is defined as

$$Z_{\rm in}(\omega) = \frac{V_{\rm in}(\omega)}{I_{\rm in}(\omega)} \tag{2}$$

where $V_{\rm in}(\omega)$ is the frequency response of the input voltage waveform and $I_{\rm in}(\omega)$ is the frequency response of the input current. The input current is determined by calculating the line integral of the circulating magnetic fields, which by the FDTD method are computed at one-half cell above the antenna feed.

A sinusoidal excitation is used to calculate the far-field radiation patterns. To obtain the absolute antenna partial directivity patterns, the following expressions are used [18]:

$$D_\theta(\theta,\phi) = 4\pi \frac{\frac{|E_\theta(\theta,\phi)|^2}{2\eta_o}}{P_{\rm input}} \tag{3}$$

$$D_\phi(\theta,\phi) = 4\pi \frac{\frac{|E_\phi(\theta,\phi)|^2}{2\eta_o}}{P_{\rm input}} \tag{4}$$

where E_θ and E_ϕ are the far-zone fields and $\eta_o = 120\pi$ is the free-space intrinsic impedance. The antenna input power is calculated from the magnitude and phase of the current and the voltage at the feed and is given by

$$P_{\rm input} = \frac{1}{2} V I^* \tag{5}$$

where * denotes complex conjugate.

III. Results

A. Wire Folded Loop Antenna Mounted on a Conducting Box

The geometry of the antenna under consideration is shown in Fig. 1. It is the vertical wire folded loop antenna mounted on a conducting box. The antenna element is centered on the handset in the x and y directions. It is fed on the left side by a coaxial cable and is short-circuited to the box on the right side. Since loop antennas are more immune to noise [18], it makes them more attractive in an interfering and fading environment, like that of mobile communications. The box dimensions are $3 \times 6 \times 10$ cm in the x, y, z directions, respectively. These dimensions are representative of a small hand-held cellular phone. The height of the antenna is 2 cm and its length is 4 cm.

The radiation patterns at 900 MHz, and the input impedance over a band of frequencies up to 5 GHz were calculated. The box dimensions in terms of wavelength at 900 MHz are approximately $0.09\lambda \times 0.18\lambda \times 0.3\lambda$. The FDTD cubical cell size is chosen to be $\Delta x = \lambda/66 = 0.5$ cm at 900 MHz and was maintained at that value for all calculations. The required problem space is $26 \times 32 \times 44$ using four PML cells and the time step is $\Delta t = 0.84 \cdot 10^{-11}$ s. The computational time is about 4 min for the radiation patterns in three major planes (1° increments) for both E_θ and E_ϕ, and 12 min for the input impedance calculation. All computations were performed on a IBM RS6000/580 workstation.

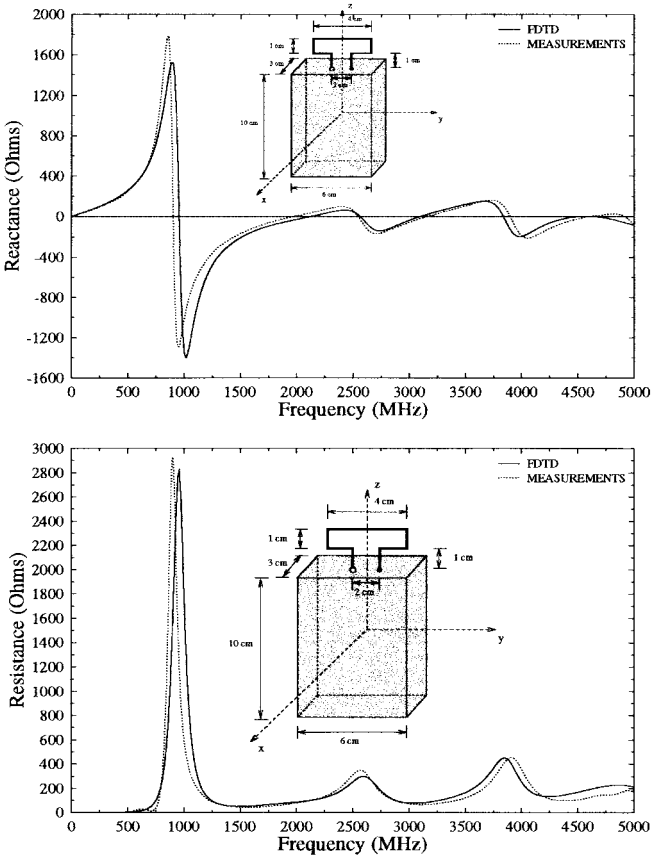

Fig. 3. Input impedance of wire folded loop antenna mounted on a conducting box.

Fig. 3 presents the predicted input impedance $Z_{\rm in} = R_{\rm in} + jX_{\rm in}$ where $R_{\rm in}$ is the input resistance and $X_{\rm in}$ is the input reactance versus frequency. The calculated results are compared with measurements and the agreement is very good in the entire frequency band. The first resonant frequency is at 945 MHz and it is of the parallel type (usually referred to as antiresonance) and it exhibits large values of resistance and reactance at resonance. The second resonance is at nearly 2150 MHz, and it is of the series type with smaller values of resistance and reactance. This type of resonance is more practical to match to conventional transmission lines, and it would be more appropriate for the new generation of PCS.

The absolute gain far-field radiation pattern for the co-polar E_θ component on the azimuth (x-y) plane is illustrated in Fig. 4, while the elevation plane patterns (x-z and y-z) are exhibited in Fig. 5. On the xy plane the pattern is almost omnidirectional, as is desirable for mobile communication system coverage. The patterns on the xz plane are symmetric, as expected, since the structure is also symmetric in this plane. The left lobe seems to be the dominant on the yz plane, and it is on the same side as the antenna feed. There is a null at 30° since the antenna is fed offset (1 cm left from the center). These results are in excellent agreement with measurements and those obtained using the NEC [10]. The measurements were performed in the ASU electromagnetic anechoic chamber (EMAC).

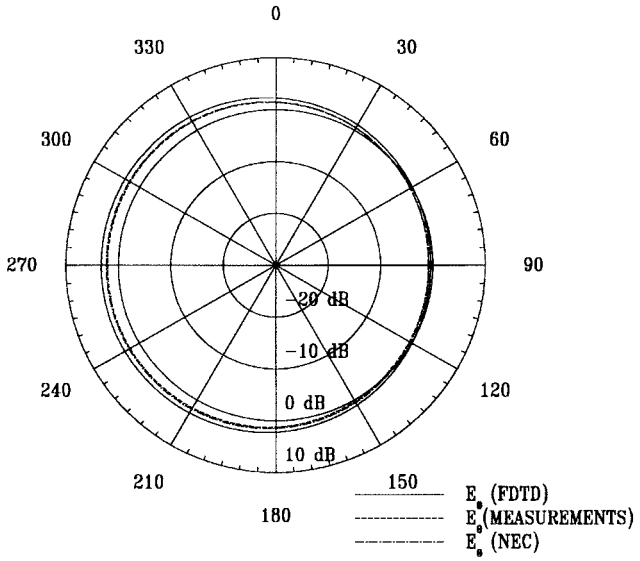

Fig. 4. Azimuth plane patterns on xy-plane of wire folded loop antenna mounted on a conducting box.

The type of resonances, and the order of occurence, exhibited in Fig. 3 are for a loop radiating element which is fed at one end and grounded to the box at the other end. The order of the resonances of Fig. 3 can be reversed by ungrounding (opening) the shorted (to the box) end of the loop. Doing this, the first resonance will be of the series type, while the second will be of the parallel type [19]. The values of the resonant frequencies remain essentially the same as those of Fig. 3. The first resonance of such a configuration would be more appropriate for the first generation (GSM or IS-54) of PCS. Thus, by grounding and ungrounding the loop at one end to the box, the same element can be used to accommodate both frequency bands, those of the existing and new generations of PCS.

B. Wire Folded Loop on a Dielectric-Coated Conducting Box

To simulate a portable telephone with a plastic case surrounding the metal chassis, the conducting box was coated with a dielectric layer with no gap between the dielectric cover and the conducting surface of the box. The dielectric permittivity of the dielectric coating is $\epsilon_r = 2.6$ and the thickness is 2.5 mm.

The dimensions of the box, the position of the element, and its dimensions were maintained the same as for the conducting case. The magnetic frill model on the top conducting surface of the box is used to model the feed of the antenna. The dielectric cover of the box was modeled using an FDTD cell of $\Delta x = \lambda/134 = 2.5$ mm, which is equal to the thickness of the dielectric cover, and the required grid size using eight PML cells is $40 \times 52 \times 76$ in the x, y, and z directions, respectively. To satisfy the Courant stability criterion, the time step $\Delta t = 0.420\,87 \cdot 10^{-11}$ s was used. The computational time is about 10 min for the radiation patterns (2680 time steps) and about 45 min for the input impedance (16 348 time steps). More time steps were used for the impedance computations than for the patterns because the impedances were computed

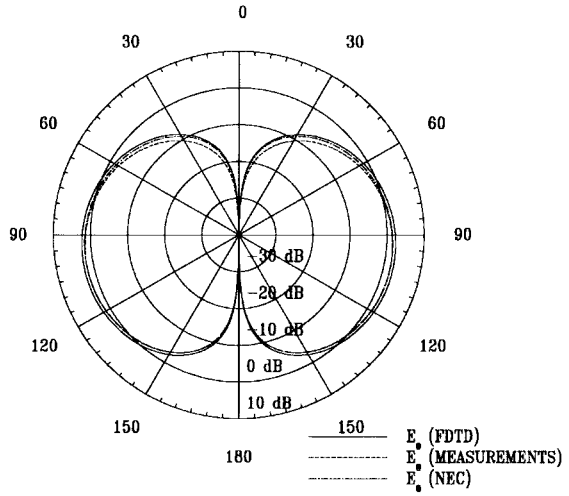

(a)

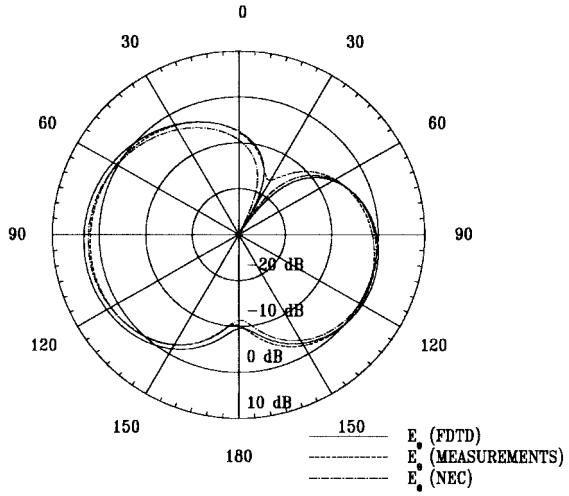

(b)

Fig. 5. Elevation plane patterns of wire folded loop antenna mounted on a conducting box. (a) xz plane. (b) yz plane.

using a pulse excitation (and the number of time steps were based on the highest frequency of its spectrum) while the patterns were computed at single frequencies.

Fig. 6 illustrates the variation of input impedance versus frequency. The predicted and measured data both indicate that the dielectric cover of the box primarily lowers the first resonant frequency (parallel type) from the original 945 MHz for the conducting box to 825 MHz for the coated box, while the second resonance (series type) is reduced from approximately 2150 to 1900 MHz. The same measurements were repeated while the box was held by a hand (referred to as *held in hand* in Fig. 6) and the values were not different from those when the box was radiating in free space, as shown in Fig. 6. This is in contrast to the detuning by the hand observed for PIFA elements [20]. The resonant frequency of the antenna can be changed by adjusting the length L of the folded loop. In both cases, with and without dielectric coating, the resonant frequency decreases as the length of the loop increases for the same loop height.

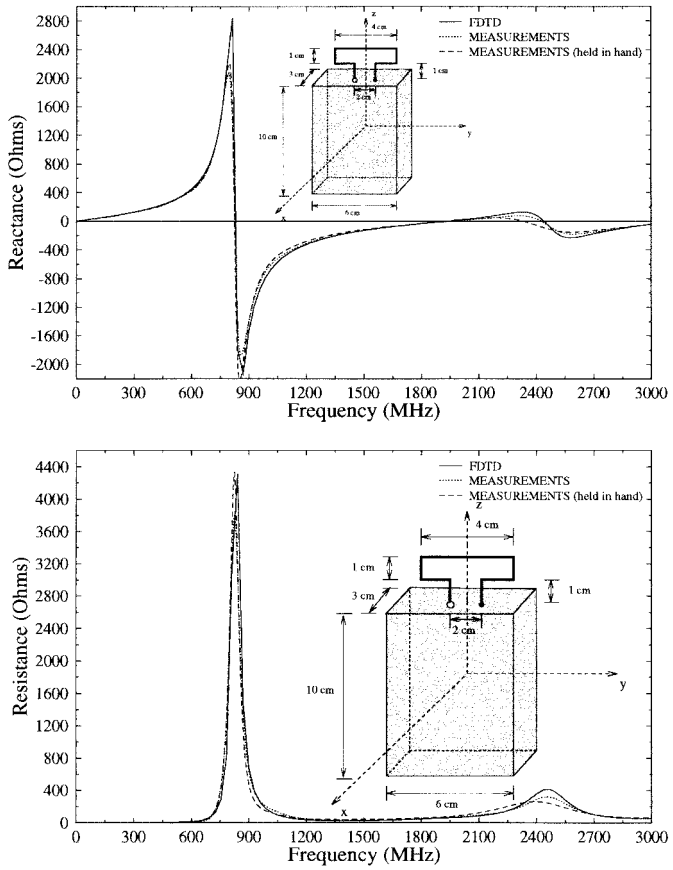

Fig. 6. Input impedance of wire folded loop antenna mounted on a dielectric covered box.

Although not presented here due to space limitations, the radiation patterns in all three planes are virtually identical between the conducting and dielectric-coated boxes. This demonstrates that the dielectric coating has very little effect on the radiation patterns of the antenna element. This is expected since the coating is relatively thin.

C. Printed Folded Loop Antenna Mounted on a Dielectric-Covered Box

The radiating element examined previously is narrowband and it is not mechanically rigid. On the other hand, planar printed elements exhibit desirable features including low cost, low weight, low profile, conformability with existing structures, and ease of fabrication and integration with active devices. The printed antenna is also attractive from a manufacturing point of view, especially for mass production using printed-circuit technology.

Because of all these attributes, the wire folded loop antenna was implemented and analyzed as a printed antenna mounted on a dielectric covered box, as shown in the inset of Fig. 7. The dielectric layer had a dielectric constant of $\epsilon_r = 2.6$ and a thickness of 2.5 mm. The antenna was printed on an isotropic, homogeneous, and lossless dielectric substrate without any groundplane on the back. The same material was used for the box cover and antenna substrate. The dimensions of the element substrate are 4 $\times$ 6 cm. The loop's length remains 4 cm, the height 2.125 cm, and the strip width is 2.5 mm.

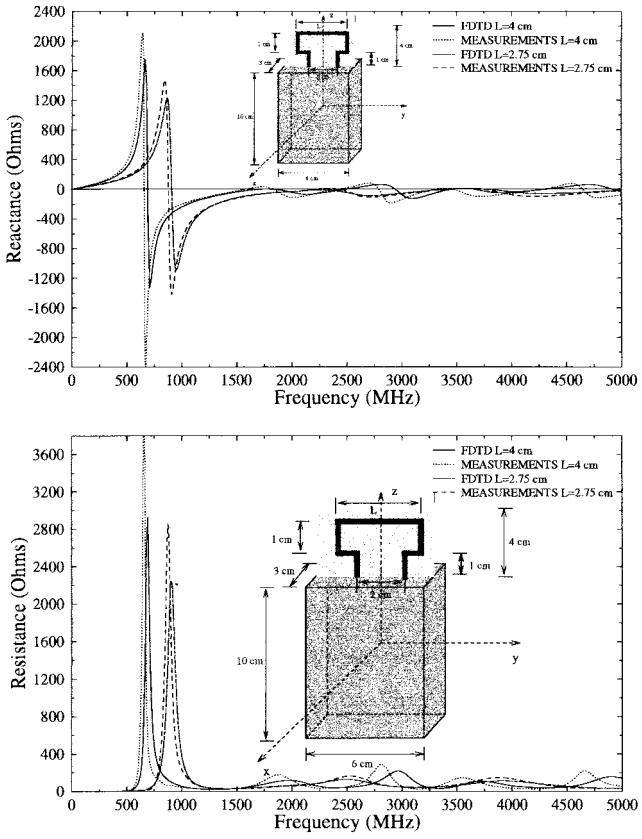

Fig. 7. Input impedance versus frequency of printed "sandwich" folded loop antenna mounted on a dielectric-covered box.

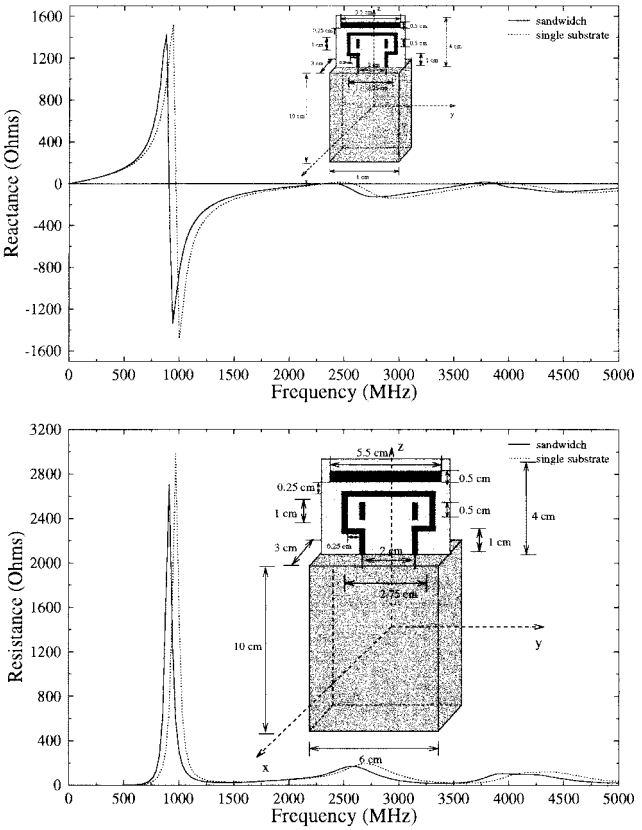

Fig. 8. Input impedance versus frequency of printed folded loop antenna mounted on a dielectric-covered box with single substrate and "sandwich" configurations.

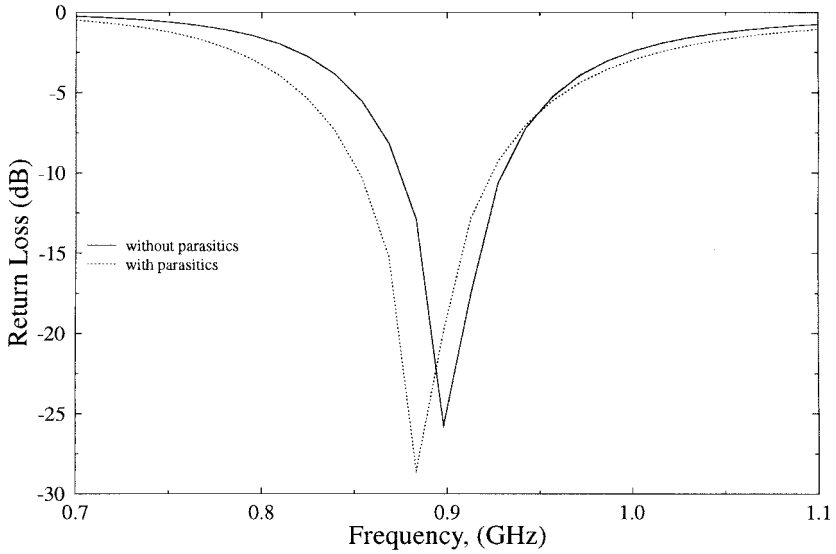

Fig. 9. Return loss versus frequency of printed folded loop antenna mounted on a dielectric-covered box with and without parasitic loading.

As shown in Fig. 7, the predicted first resonant frequency is 682 MHz and it is much smaller than that of the wire element, even though the loop dimensions are the same. The calculated results are in good agreement with the measurements since the first measured resonant frequency is 662 MHz. By decreasing the length of the antenna, the resonant frequency can be increased. To illustrate this, the antenna length was decreased to 2.75 cm. The response of such a design is also depicted in Fig. 7 where the FDTD predicted resonant frequency is now 905 MHz. The antenna bandwidth is still narrow.

Recently, extensive research has been devoted to the bandwidth problem and considerable progress has been made. The problem of increasing the bandwidth of printed antenna elements has received some attention in the literature [21]–[24], and it appears that parasitic elements play an important role. This approach was also used to increase the bandwidth of the printed folded loop antenna, as illustrated in the inset of Fig. 8. The parasitic elements used in this case are two small strips with dimensions 2.5 $\times$ 5.0 mm inside the folded loop and a long strip with dimensions 0.5 $\times$ 5.5 cm outside the loop. The separation between the antenna and the upper parasitic element is 2.5 mm. The size of the dielectric substrate is still 4 $\times$ 6 cm.

The antenna element with and without parasitics is covered with a dielectric layer of the same dimensions as the substrate with permittivity $\epsilon_r = 2.6$ and 2.5 mm thickness. The entire antenna structure takes the form of a *sandwich*. This surface works as superstrate loading and causes a shift in resonant frequency as shown in Fig. 8, where the input impedance versus frequency for a single substrate and a sandwich configuration are plotted. The radiation patterns of the printed loop, with and without parasitics and with and without the superstrate cover, maintain their desirable characteristics, and they have basically the same shape as those of the wire loop shown in Figs. 4 and 5. They also compare favorably with measurements. However, because of space limitations, they are not included here, but can be found in [17]. In addition to the frequency tuning, the double dielectric cover protects the printed antenna from environmental conditions (corrosion) and gives the antenna an attractive appearance.

The FDTD cell-size requirement in this case is $\Delta x = \lambda/268 = 1.25$ mm at 900 MHz and the number of FDTD cells along the x, y and z directions are 52 $\times$ 76 $\times$ 162, respectively. The Courant stability criterion is used to select the time-step $\Delta t = 0.207\,296 \cdot 10^{-11}$ s to insure numerical stability. The antenna is fed on the left side by a coaxial cable, which is simulated by the magnetic-frill model on the top conducting surface of the box. The CPU time is 42 min (5360 time steps) for the radiation patterns and about 135 min for the input impedance (16 384 time steps).

To examine the effects of the strip width on the resonant frequency and the bandwidth, the return loss versus frequency was computed and is displayed in Fig. 9. This figure shows that for a 2 : 1 VSWR, the bandwidth without parasitics is 5.75% and with parasitic loading the bandwidth is 8.55%, an increase of about 3%. Industry specifications for voice and data transmission require a bandwidth of about 7%. The amplitude radiation patterns in all planes are essentially unaffected by the strip width or parasitic loading.

IV. Conclusion

A vertical folded loop antenna for existing mobile communications systems has been introduced and analyzed. The antenna is mounted on a conducting box, with and without dielectric coating, to simulate a cellular telephone. The FDTD method was used to analyze the radiation characteristics (input impedance, radiation patterns on principal planes) of this antenna. PML absorbing boundary conditions were implemented to truncate the computational domain for a practical three-dimensional antenna.

The folded loop was implemented both as a wire and as a printed antenna to exploit the advantages of the printed-circuit technology. It has been shown that the FDTD method is a very powerful tool for analyzing both antenna configurations. The printed element exhibits much lower input impedance,

especially at resonance, than those of the wire elements. Parasitic loading was used to enhance the bandwidth of the printed antenna, and the design parameters of this configuration were analyzed. The same element can be used to accommodate both frequency bands of the existing and new generation of PCS by grounding and ungrounding the loop at one end. The calculated results were compared with measurements and those obtained from the NEC and all were in very good agreement. These results meet all the design requirements for existing and future mobile communication systems.

REFERENCES

[1] M. B. Pautet and M. Mouly, *The GSM System for Mobile Communications*. Paris, France: 1992.

[2] D. J. Goodman, "Second generation wireless information networks," *IEEE Trans. Veh. Technol.*, vol. 40, pp. 366–374, May 1991.

[3] R. Luebbers, L. Chen, T. Uno, and S. Adachi, "FDTD calculation of radiation patterns, impedance, and gain for a monopole antenna on a conducting box," *IEEE Trans. Antennas Propagat.*, vol. 40, pp. 1577–1583, Dec. 1992.

[4] M. A. Jensen and Y. Rahmat-Samii, "Performance analysis for handheld transceivers using FDTD," *IEEE Trans. Antennas Propagat.*, vol. 42, pp. 1106–1113, Aug. 1994.

[5] T. Taka and K. Tsunekawa, "Performance analysis of a built-in planar inverted F antenna for 800 MHz band portable radio units," *IEEE J. Select. Areas Commun.*, vol. 5, pp. 921–929, June 1987.

[6] J. Berenger, "A perfectly matched layer for the absorption of electromagnetic waves," *J. Comput. Phys.*, no. 114, pp. 185–200, Oct. 1994.

[7] D. S. Katz, E. T. Thiele, and A. Taflove, "Validation and extension to three dimensions of the berenger PML absorbing boundary condition for FD-TD meshes," *IEEE Microwave Guided Wave Lett.*, vol. 4, pp. 268–270, Aug. 1994.

[8] R. Mittra and U. Pekel, "A new look at the perfectly matched layer (PML) concept for the reflectionless absorption of electromagnetic waves," *IEEE Microwave Guided Wave Lett.*, vol. 5, pp. 84–86, Mar. 1995.

[9] W. V. Andrew, C. A. Balanis, and P. A. Tirkas, "A comparison of the Berenger perfectly matched layer and the Lindman higher-order ABC's for the FDTD method," *IEEE Microwave Guided Wave Lett.*, vol. 5, pp. 192–194, June 1995.

[10] C. J. Burke and A. J. Poggio, *Numerical Elecromagnetics Code (NEC): User's Manual*, Lawrence Livermore Nat. Lab., Livermore, CA, Jan. 1981.

[11] A. Taflove, *Computational Electrodynamics: The Finite-Difference Time-Domain Method*. Boston, MA: Artech, 1995.

[12] P. A. Tirkas and C. A. Balanis, "Finite-difference time-domain method for antenna radiation," *IEEE Trans. Antennas Propagat.*, vol. 40, pp. 334–340, Mar. 1992.

[13] C. Wu, K. L. Wu, Z. Q. Bi, and J. Litva, "Accurate characterization of planar printed antennas using FDTD method," *IEEE Trans. Antennas Propagat.*, vol. 40, pp. 526–535, May 1992.

[14] H. S. Tsai and R. A. York, "FDTD analysis of CPW-fed folded-slot and multiple-slot antennas on thin substrates," *IEEE Trans. Antennas Propagat.*, vol. 44, pp. 217–227, Feb. 1996.

[15] C. A. Balanis, *Advanced Enginering Electromagnetics*. New York: Wiley, 1989.

[16] A. Taflove and M. E. Brodwin, "Numerical solution of steady-state electromagnetic scattering problems using the time-dependent Maxwell's equations," *IEEE Trans. Microwave Theory Tech.*, vol. 23, pp. 623–630, Aug. 1995.

[17] K. D. Katsibas, "Analysis and design of mobile antennas for handheld units," Masters' thesis, Arizona State University, Tempe, AZ, Aug. 1996.

[18] C. A. Balanis, *Antenna Theory: Analysis and Design*, 2nd ed. New York: Wiley, 1996

[19] C. A. Balanis, K. D. Katsibas, P. A. Tirkas, and C. R. Birtcher, "Loop antenna for mobile and personal communication systems," in *IEEE 47th Annu. Int. Veh. Technol. Conf.*, Phoenix, AZ, May 1997, pp. 452–454.

[20] M. A. Jensen and Y. Rahmat-Samii, "EM interaction of handset antennas and a human in personal communications," *Proc. IEEE*, vol. 83, pp. 5–17, Jan. 1995.

[21] H. Y. Yang and N. G. Alexopoulos, "Gain enhancement methods for printed circuit antennas through multiple superstrates," *IEEE Trans. Antennas Propagat.*, vol. AP-35, pp. 860–863, July 1987.

[22] L. P. B. Katehi and N. G. Alexopoulos "On the modeling of electromagnetically coupled microstrip antennas-the printed strip dipole," *IEEE Trans. Antennas Propagat.*, vol. AP-32, pp. 1179–1186, Nov. 1984.

[23] R. Q. Lee and K. F. Lee, "Gain enhancement of microstrip antennas with overlaying parasitic directors," *Electron. Lett.*, vol. 24, no. 11, pp. 656–658, May 1988.

[24] C. Wood, "Improved bandwidth of microstrip antennas using parasitic elements" *Proc. Inst. Elect. Eng.—Microwaves Opt. Antennas*, vol. 127, pt. H, no. 4, pp. 231–234, Aug. 1980.

Konstantinos D. Katsibas was born in Athens, Greece. He received the Diploma in electrical and computer engineering from the National Technical University, Athens, in June 1993.

In August 1993 he joined Arizona State University, Tempe. From August 1993 through June 1996 he was under a Greek Government Fellowship. From January 1995 until May 1996 he worked as a Graduate Research Assistant in the Telecommunications Research Center of Arizona State University.

Constantine A. Balanis (S'62–M'68–SM'74–F'86), for photograph and biography, see this issue, p. 259.

Panayiotis A. Tirkas (SM'89–M'93) was born in Nicosia, Cyprus. He received the B.S. and M.S. degrees in electrical engineering from the University of Kansas, Lawrence, in 1987 and 1989, respectively, and the Ph.D. degree in electrical engineering from Arizona State University, Tempe, in 1993.

From 1982 to 1987, he was under a Fulbright Exchange Scholarship at University of Kansas, Lawrence. From 1988 to 1989 he worked as a Graduate Research Assistant at the Remote Sensing Laboratory, University of Kansas, Lawrence. From 1989 to 1993 he was a Graduate Research Associate at the Telecommunications Research Center, Arizona State University, Tempe, under a fellowship from the Aileen S. Andrew Foundation. He was an Assistant Research Engineer at the Telecommunications Research Center, Arizona State University, from 1993 to 1997. Currently, he is an Engineering Specialist at Space Systems/Loral, Palo Alto, CA, where he is invlolved in the analysis, design, and testing of satellite antenna feeds and RF circuits. His current interests include the application of finite-element and mode-matching methods for the analysis and design of satellite antenna feeds and RF payloads, and in multipactor testing of satellite antenna components.

Dr. Tirkas coordinated the Advanced Helicopter Electromagnetics consortium and conducted research on propagation models for mobile statellite communications, high-intensity radiated field (HIRF) penetration in aircraft, and electrical characterization of electronic packages at Arizona State University (1993–1997). He is a member of Tau Beta Pi and Sigma Xi.

Craig R. Birtcher, for photograph and biography, see this issue, p. 259.